JIPB Journal of Integrative Plant Biology

Research Article
https://doi.org/10.1111/jipb.13460

ESCRT-III component OsSNF7.2 modulates leaf rolling by trafficking and endosomal degradation of auxin biosynthetic enzyme OsYUC8 in rice

Liang Zhou[1,2†], Saihua Chen[1,3†], Maohong Cai[1], Song Cui[1], Yulong Ren[2], Xinyue Zhang[2], Tianzhen Liu[2], Chunlei Zhou[1], Xin Jin[2], Limin Zhang[2], Minxi Wu[2], Shuyi Zhang[2], Zhijun Cheng[2], Xin Zhang[2], Cailin Lei[2], Qibing Lin[2], Xiuping Guo[2], Jie Wang[2], Zhichao Zhao[2], Ling Jiang[1], Shanshan Zhu[2*] and Jianmin Wan[1,2*]

1. State Key Laboratory for Crop Genetics and Germplasm Enhancement, Jiangsu Plant Gene Engineering Research Center, Nanjing Agricultural University, Nanjing 210095, China
2. National Key Facility for Crop Gene Resources and Genetic Improvement, Institute of Crop Sciences, Chinese Academy of Agricultural Sciences, Beijing 100081, China
3. Jiangsu Key Laboratory of Crop Genomics and Molecular Breeding/Key Laboratory of Plant Functional Genomics of the Ministry of Education/Jiangsu Key Laboratory of Crop Genetics and Physiology, Agricultural College of Yangzhou University, Yangzhou 225009, China

[†]These authors contributed equally to this work.
*Correspondences: Shanshan Zhu (zhushanshan@caas.cn), Jianmin Wan (wanjm@njau.edu.cn, Dr. Wan is fully responsible for the distributions of the materials associated with this article)

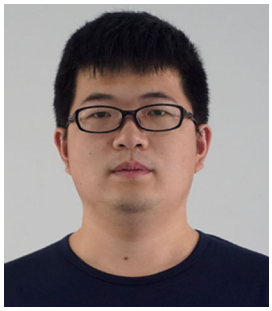

Liang Zhou

Jianmin Wan

ABSTRACT

The endosomal sorting complex required for transport (ESCRT) is highly conserved in eukaryotic cells and plays an essential role in the biogenesis of multivesicular bodies and cargo degradation to the plant vacuole or lysosomes. Although ESCRT components affect a variety of plant growth and development processes, their impact on leaf development is rarely reported. Here, we found that OsSNF7.2, an ESCRT-III component, controls leaf rolling in rice (*Oryza sativa*). The *Ossnf7.2* mutant *rolled leaf 17* (*rl17*) has adaxially rolled leaves due to the decreased number and size of the bulliform cells. *OsSNF7.2* is expressed ubiquitously in all tissues, and its protein is localized in the endosomal compartments. OsSNF7.2 homologs, including OsSNF7, OsSNF7.3, and OsSNF7.4, can physically interact with OsSNF7.2, but their single mutation did not result in leaf rolling. Other ESCRT complex subunits, namely OsVPS20, OsVPS24, and OsBRO1, also interact with OsSNF7.2. Further assays revealed that OsSNF7.2 interacts with OsYUC8 and aids its vacuolar degradation. Both *Osyuc8* and *rl17 Osyuc8* showed rolled leaves, indicating that OsYUC8 and OsSNF7.2 function in the same pathway, conferring leaf development. This study reveals a new biological function for the ESCRT-III components, and provides new insights into the molecular mechanisms underlying leaf rolling.

Keywords: bulliform cell, leaf rolling, *OsSNF7.2*, *OsYUC8*, rice (*Oryza sativa*), vacuolar degradation

Zhou, L., Chen, S., Cai, M., Cui, S., Ren, Y., Zhang, X., Liu, T., Zhou, C., Jin, X., Zhang, L., Wu, M., Zhang, S., Cheng, Z., Zhang, X., Lei, C., Lin, Q., Guo, X., Wang, J., Zhao, Z., Jiang, L., Zhu, S., and Wan, J. (2023). ESCRT-III component OsSNF7.2 modulates leaf rolling by trafficking and endosomal degradation of auxin biosynthetic enzyme OsYUC8 in rice. J. Integr. Plant Biol. **00:** 1–16.

INTRODUCTION

Rice (*Oryza sativa*) is the most important crop in the world, providing the main source of calories for more than half of the world's population (Sasaki Takuji, 2000). Rice yield is affected by the photosynthetic efficiency of the plant, which is modulated by its leaf morphology (Xu et al., 2018). Under light and water stress, plants use leaf rolling to protect

against photodamage and reduce water loss (Moon and Hake, 2011). Many elements have been found to control leaf rolling, including the leaf polarity, bulliform cells, sclerenchymatous cells, and the level of cuticle development (Xu et al., 2018). In monocotyledons such as rice, bulliform cells are located in the adaxial leaf epidermis to control rolling (Itoh et al., 2005). Many genes were identified as regulating leaf rolling by altering the size or number of bulliform cells. The overexpression of *Abaxially Curled Leaf 1* (*ACL1*) or *ACL2* increases the number and size of bulliform cells in rice leaves, resulting in the abaxial curling of the leaf blades (Li et al., 2010). The decreased expression of *RL14*, which encodes a 2OG-Fe (II) oxygenase, reduces the size of the bulliform cells and causes adaxial leaf rolling (Fang et al., 2012). The overexpression of *ZINC FINGER HOMEODOMAIN 1* (*OsZHD1*) or *OsZHD2* causes abaxial leaf rolling by increasing the numbers of bulliform cells (Xu et al., 2014). Rice Outermost Cell-Specific 5 (ROC5) interacts with URL1/ROC8 and TPL2 to form a repressor complex that regulates leaf rolling by negatively regulating the number and size of bulliform cells (Xu et al., 2021). The variously named CONSTITUTIVELY WILTED 1 (COW1)/NARROW LEAF 7 (NAL7)/OsYUC8, a homolog of YUCCA in *Arabidopsis thaliana*, is an enzyme involved in auxin biosynthesis (Woo et al., 2007). OsYUC8 control leaf rolling by regulating the size of bulliform cells. Although OsYUC8 functions as an enzyme for auxin biosynthesis, its underlying mechanism controlling leaf rolling is unclear.

The endomembrane system, consisting of functionally distinct membrane-bound organelles, plays a significant role in plant growth and development (Fan et al., 2015). Multivesicular bodies (MVBs), which are late-endosomal organelles, act as an intermediate station for cargo degradation, intracellular recycling, and secretion (Winter and Hauser, 2006). The endosomal sorting complexes required for transport (ESCRT) are highly conserved in eukaryotic cells, and play essential roles in biogenesis of the MVBs and cargo degradation in the vacuole or lysosome (Henne et al., 2011; Gao et al., 2017). They consist of several functionally different subcomplexes, including ESCRT-0, -I, -II, and -III, as well as several accessory components (Henne et al., 2011; Gao et al., 2017).

Partial ESCRT components were recently identified in plants. The *Arabidopsis* ESCRT-I subunit VPS23A performs a crucial role in the abscisic acid (ABA) signaling pathway by affecting the vacuole-mediated degradation of PYR1/PYLs (Yu et al., 2016). ESCRT-II subunit VPS36 in *Arabidopsis* regulates MVB biogenesis and endosomal sorting for the degradation of membrane cargoes (Wang et al., 2017). The ESCRT-III accessory proteins CHMP1A and CHMP1B influence embryo and seedling development by regulating MVB biogenesis and the vacuolar sorting of auxin transporters in *Arabidopsis* (Spitzer et al., 2009). A plant-specific ESCRT component, FREE1, was found to play multiple functional roles in vacuolar protein trafficking and organelle biogenesis, as well as autophagic degradation (Gao et al., 2014; Gao et al., 2015). In rice, knocking out *OsVPS22* expression caused white-core grains and seedling lethality, but the endosomal sorting of the *Osvps22* mutants remains unknown (Zhang et al., 2013). The ESCRT components therefore affect various processes in plant growth and development, but were not previously reported to influence leaf rolling, and more research is required to determine the precise activities of the ESCRT components in rice.

In this study, we report that the ESCRT-III component OsSNF7.2 controls leaf rolling in rice. The *OsSNF7.2* gene is constitutively expressed in rice, and its protein OsSNF7.2 is localized to the endosomal compartment. OsSNF7.2 performs as a homodimer or heterodimer with its homologs OsSNF7, OsSNF7.3, and OsSNF7.4, the mutation of which did not cause leaf rolling. OsSNF7.2 can physically interact with OsYUC8 to affect its vacuolar degradation. *Osyuc8* and *rolled leaf 17* (*rl17*)/*Ossnf7.2 Osyuc8* also have rolled leaves, which indicated OsYUC8 and OsSNF7.2 function in the same pathway controlling leaf rolling. Our findings reveal a novel biological role for the ESCRT-III complex in regulating leaf rolling.

RESULTS

The *rl17* mutant has rolled leaves due to the reduced size and number of its bulliform cells

To study the molecular mechanism of rice leaf rolling, a rolled leaf mutant, *rl17*, was isolated from a gamma ray mutagenesis of the *japonica* rice variety Asominori. Compared with the wild-type, the *rl17* mutant possessed adaxially rolled and darker green leaves, particularly at the tillering stage (Figure 1A–C). The leaf-rolling index (LRI) was used to quantify the extent of leaf rolling (Shi et al., 2007). The flag leaf LRI values for the *rl17* mutant at heading were approximately 30% (Figure 1D). The flag leaf width of the mutant was 20% less than that of the wild-type (Figure 1E). Toluidine blue O was used to stain the bulliform cells of the wild-type and *rl17* plants, revealing fewer and smaller purple-stained bulliform cell layers in the *rl17* mutant (Figure 1F, G). Furthermore, paraffin sections showed that the number and size of bulliform cells were reduced in the *rl17* mutant, with no significant difference observed in other cellular structures (Figure 1H–M). Significant changes of other agronomic traits were observed in the *rl17* mutant, including the plant height, spike length, 1 000-grain weight, seed-setting rate, and grain width (Table S1).

Map-based cloning of *RL17*

Using 24 F_2 mutant individuals from a cross between the *rl17* mutant and the *indica* cultivar IR24, the *RL17* locus was initially located within a 2.43-Mb physical interval flanked by markers *DF53* and *NJ9*-5 on chromosome 9, which was narrowed to a 49-kb region between markers *JY-17* and *JY-15* using 1 850 mutant individuals from a population of F_2-derived F_3 ($F_{2:3}$) lines (Figure 2A). This region contains six putative open reading frames, and a sequence analysis

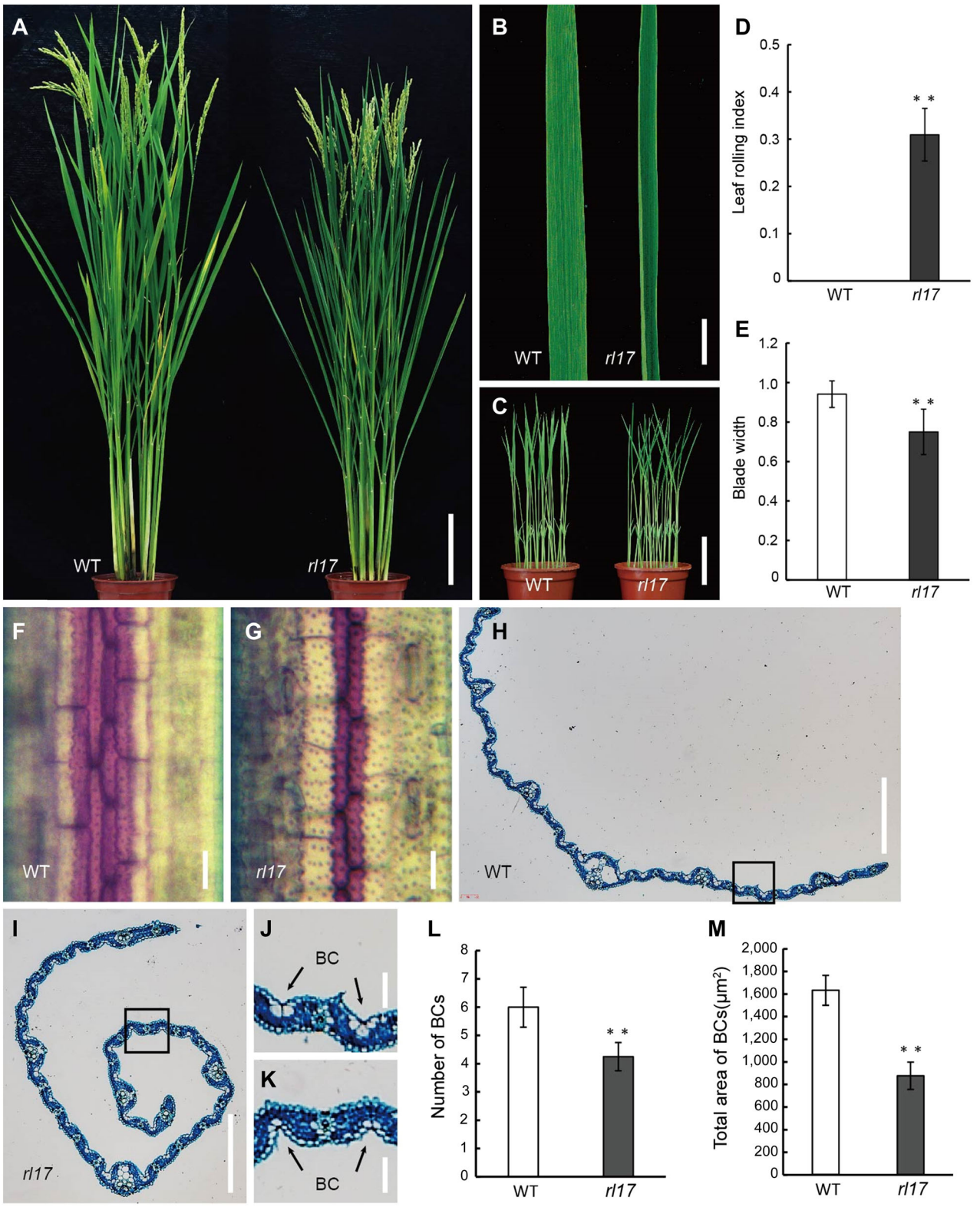

Figure 1. The *rl17* mutant phenotype

(**A**) Plant stature of the wild-type (WT) and *rl17* mutant plants at maturity. Bar, 10 cm. (**B**) Adaxial sides of flag leaf blades from the WT and *rl17* mutant at maturity. Bar, 1 cm. (**C**) Seven-d-old WT and *rl17* mutant seedlings. Bar, 4 cm. (**D**) and (**E**) Leaf rolling index (LRI; D) and blade widths (E) of the flag leaves of the WT and *rl17* mutant plants ($n = 20$, $^{**}P < 0.01$; Student's *t*-test). (**F**) and (**G**) Toluidine blue O staining of bulliform cells from the adaxial epidermal peels abutting the small veins of 30-d-old WT and *rl17* mutant plants. Bars, 100 μm. (**H**) and (**I**) Cross-sections of the WT and *rl17* mutant leaves from 30-d-old plants. Bars, 500 μm. (**J**) and (**K**) Close-up images of bulliform cells (labeled as BC) in the adaxial epidermal layer (inset (H) and (I)). Bars, 100 μm. (**L**) and (**M**) Statistical analysis of the number (L) and total area (M) of the bulliform cells. Data are means ± *SD* ($n = 10$, $^{**}P < 0.01$; Student's *t*-test).

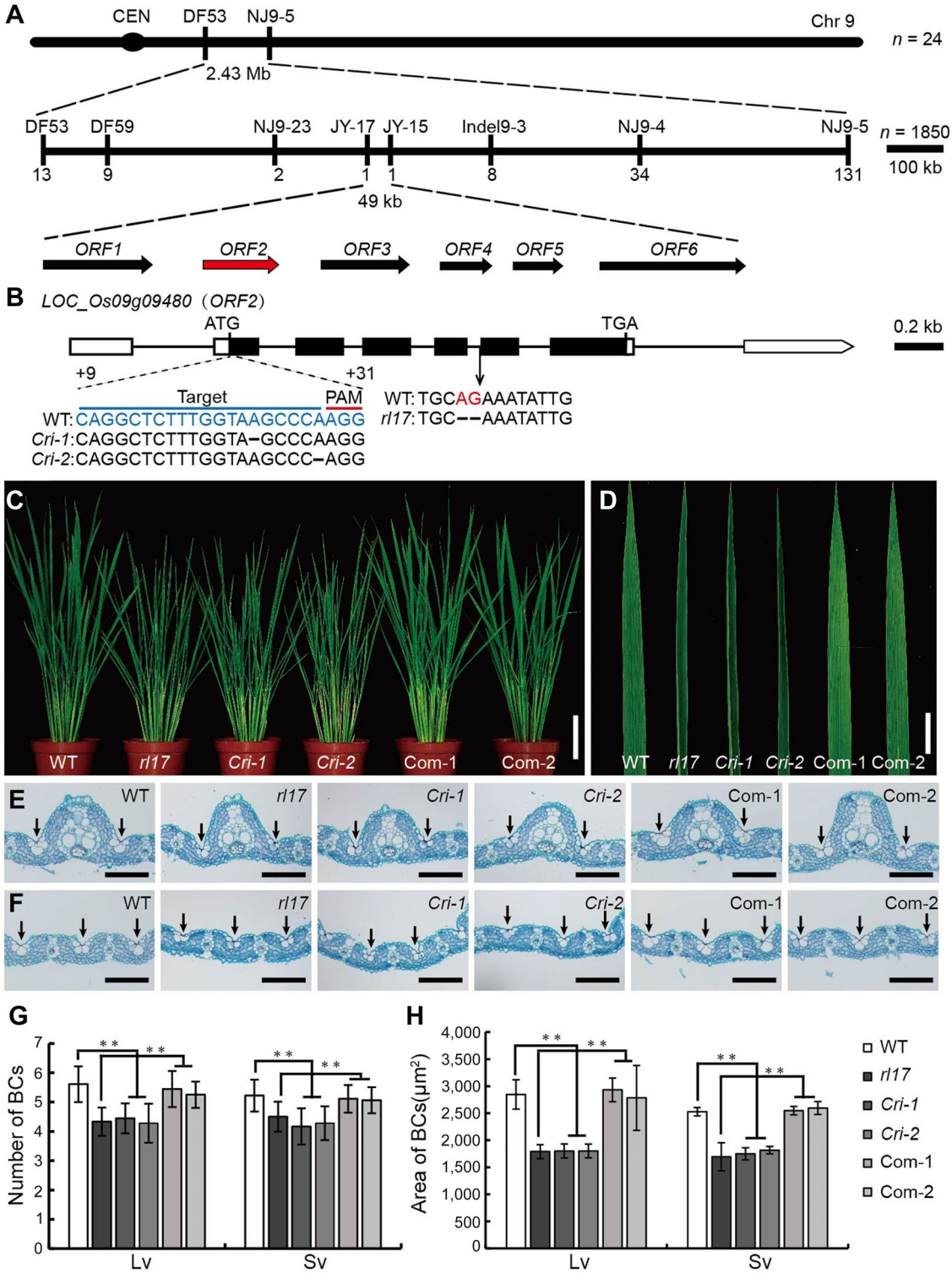

Figure 2. Map-based cloning of *RL17* and the complementation of *rl17*

(**A**) Fine mapping of the *RL17* locus. The candidate gene was narrowed to a 49-kb region between markers *JY-17* and *JY-15* on chromosome 9. Molecular markers and numbers of recombinants are indicated. (**B**) Gene structure and mutation site of *RL17*. The *RL17* gene comprises eight exons (closed boxes) and seven introns (lines). ATG and TGA are the start and stop codons, respectively. A 2-bp deletion in *rl17* caused a premature termination of translation. (**C**) and (**D**) Phenotypes of the wild-type (WT), *rl17*, knockout lines and complemented plants. A 5.1-kb WT genomic segment of *RL17* rescued the narrow, rolled leaf phenotype. The guide RNA targeting sites and protospacer adjacent motifs (PAMs) are indicated in (**B**). Bars, 10 cm (**C**), 1 cm (**D**). (**E**) and (**F**) Leaf cross-sections showing bulliform cells near large veins (**E**) and small veins (**F**) in 30-d-old WT, *rl17* mutant, and transgenic plants. The black arrows indicate bulliform cells. Bars, 100 μm. (**G**) and (**H**) Statistical analysis of the number (**G**) and area (**H**) of bulliform cells in the WT, *rl17* mutant, and transgenic plants. Data are presented as means ± *SD* ($n = 10$, $^{**}P < 0.01$; Student's *t*-tests).

revealed a 2-bp deletion in the fifth intron of the *LOC_Os09g09480* gene in the *rl17* mutant, causing incorrect intron splicing and generating a 46-bp deletion in the sixth exon (coding sequence), which resulted in premature translation (Figure 2B).

To verify that the mutation of *LOC_Os09g09480* was responsible for the rolled leaf phenotype, a 5.1-kb genomic fragment amplified from Asominori, including the full coding region of *LOC_Os09g09480* and its native promoter sequences, was introduced into the *rl17* mutant. All positive transgenic lines displayed a rescued leaf phenotype (Figure 2C, D). Consistent with this, *LOC_Os09g09480*-knockout mutants generated in Asominori using clustered regularly interspaced palindromic repeats (CRISPR)/CRISPR-associated protein 9 (Cas9) exhibited rolled leaves (Figure 2B–D). Cross section and quantitative analyses of the wild-type and CRISPR-*RL17* leaves confirmed that the curled leaves are caused by the reduced number and size of bulliform cells in *rl17* (Figure 2E–H). These findings confirm that *LOC_Os09g09480* is the *RL17* gene.

RL17 encodes an SNF7 subunit of the ESCRT-III complex, which localizes in the endosomal compartment

A Basic Local Alignment Search Tool (BLAST) search indicated that *LOC_Os09g09480* encodes a predicted protein of 24 kDa containing a SNF7 domain, a subunit of the ESCRT-III complex. According to the phylogenetic analysis, *LOC_Os09g09480* was designated as *OsSNF7.2* and the other two *SNF7* paralogs with high sequence similarity to *OsSNF7.2* were also named as OsSNF7.3 and OsSNF7.4 in this study (Figure S1A). A quantitative real-time polymerase chain reaction (qRT-PCR) analysis revealed that *RL17*/*OsSNF7.2* is expressed ubiquitously in all tissues, with relatively higher expression levels in the stems, leaves, and leaf sheaths (Figure 3A). A messenger RNA (mRNA) *in situ* hybridization assay showed that *OsSNF7.2* was specifically expressed in the leaf mesophyll cells and leaf sheaths (Figure 3B, C). The β-glucuronidase (GUS) staining of $Pro_{OsSNF7.2}$:*GUS* transgenic plants showed that *OsSNF7.2* was expressed in all tissues, consistent with the qRT-PCR results (Figure 3E–I). The transient co-expression of OsSNF7.2-GFP (green fluorescent protein) with the late-endosome marker mCherry-VSR2 in rice protoplasts showed that OsSNF7.2 is localized in the endosomal compartment (Figure 3J). These results indicated that OsSNF7.2 is a late-endosome-localized protein.

OsSNF7.2 interacts with its homologs

Previous studies have demonstrated that SNF7 can form a self-multimer complex that functions in vacuolar trafficking in animal and yeast cells (Winter and Hauser, 2006). A comparable complex was functionally characterized in *Arabidopsis*, in which two homologous proteins formed heterodimers (Richardson et al., 2011). There are many genes containing SNF7 domains in the rice genome, and a phylogenetic analysis indicated that *OsSNF7.2* shared high similarity with its homologs (Figure S1A, B). To test whether the functional mode of OsSNF7.2 in rice is similar to SNFs in animal and yeast cells, yeast two-hybrid (Y2H) assays were performed and strong interactions between OsSNF7.2 and its rice homologs were identified (Figure 4A). These interactions were further verified using *in vivo* co-immunoprecipitation (Co-IP) assays in rice protoplasts (Figure 4B), and bimolecular fluorescent complementation (BiFC) (Figure 4C) and luciferase complementation imaging (LCI) assays (Figure S2) in *Nicotiana benthamiana* leaves. Further Y2H assays confirmed that OsSNF7.2 can also interact with multiple subunits of the ESCRT complex, including OsVPS20, OsVPS24, and OsBRO1 (Figure S3).

To investigate the function of OsSNF7.2 homologs in the regulation of leaf rolling, knockout mutants were generated in the Asominori background using CRISPR/Cas9 genome editing. These mutant lines did not show leaf rolling (Figure S4), thus implying a specific role for *OsSNF7.2* in regulating leaf rolling in rice.

OsSNF7.2 interacts with OsYUC8

In order to investigate how *OsSNF7.2* controls leaf morphology, the expression levels of the genes related to leaf rolling were checked in the *rl17* mutant. No difference in the expression of these genes was found between the wild-type and *rl17* (Figure S5).

Next, immunoprecipitation–mass spectrometry (IP–MS) assays were performed using rice protoplasts expressing OsSNF7.2-GFP, and the auxin biosynthetic enzyme OsYUC8 was screened as a potential interacting partner (Figure S6). In *in vivo* Co-IP assays, OsYUC8-Flag was co-immunoprecipitated by OsSNF7.2-GFP but not free GFP (Figure 5A). The interaction was verified using *in vivo* LCI assays and BiFC assays in *N. benthamiana* leaf epidermal cells (Figure 5B, C). The interaction between OsSNF7.2 and OsYUC8 was localized in the late endosomes, which is consistent with the subcellular location of OsSNF7.2 (Figure 5C). Together, these results confirm that OsSNF7.2 can physically interact with OsYUC8. Co-IP assays were also performed to further investigate whether OsYUC8 can interact with the OsSNF7.2 homologs, revealing that OsYUC8 can also interact with OsSNF7, OsSNF7.3, and OsSNF7.4 (Figure S7). We also found that, in addition to OsYUC8, OsYUC1.2, OsYUC2, OsYUC3, OsYUC4, OsYUC5, OsYUC6, and OsYUC7 can also physically interact with OsSNF7.2 (Figure S8).

The *rl17* mutation affects the degradation of OsYUC8-GFP

Previous studies in mammals and yeast have shown that the ESCRT complex functions in trafficking ubiquitinated endocytic cargo from the endosome to the lysosome for degradation (Henne et al., 2011); thus, we speculated that OsYUC8 may be the transport target of the ESCRT-III component

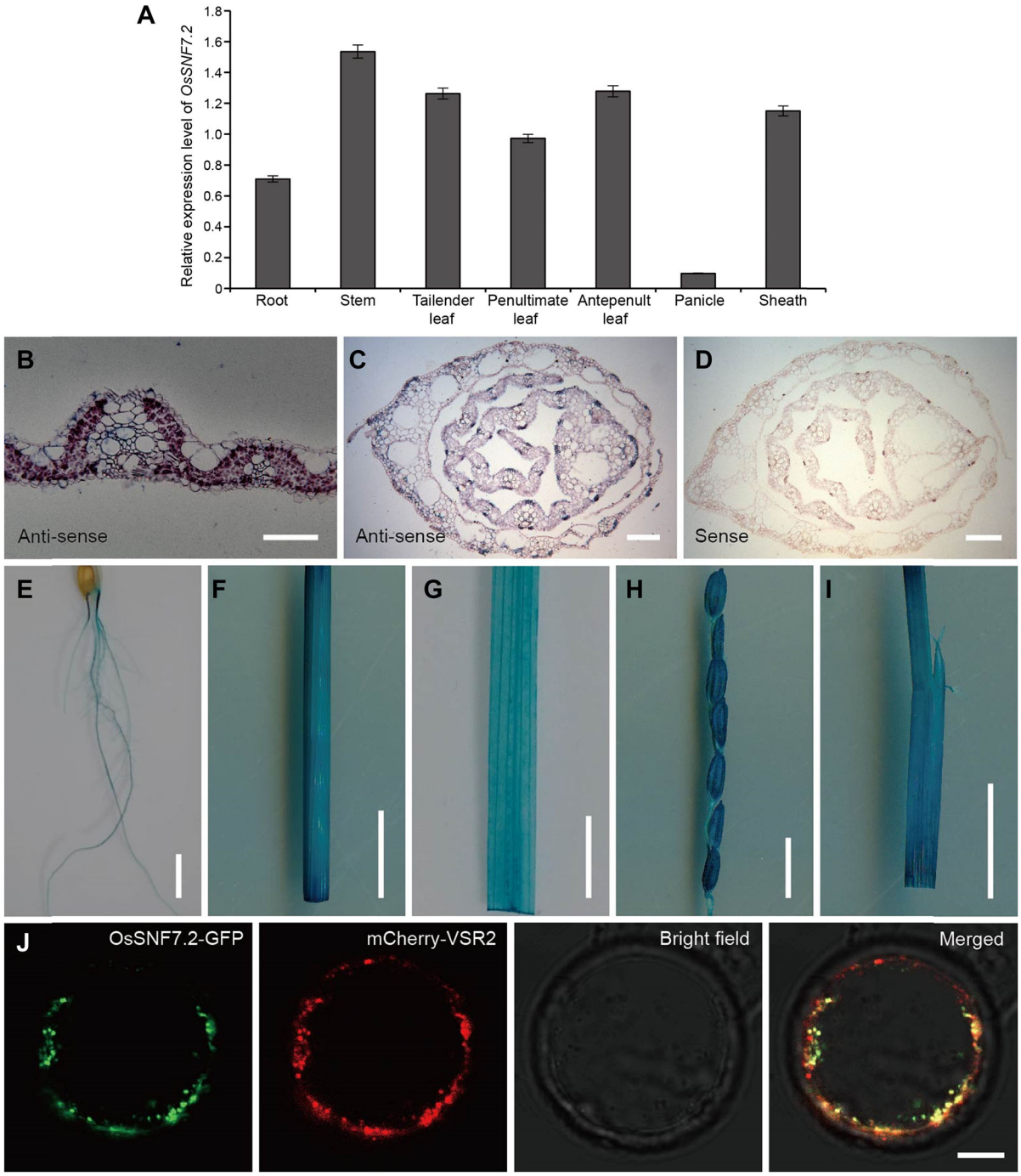

Figure 3. Expression pattern analysis of *OsSNF7.2* and the subcellular localization of the OsSNF7.2 protein

(**A**) Expression pattern analysis of *OsSNF7.2* in different plant tissues. Values are means ± *SD* ($n = 3$). (**B**–**D**) *In situ* hybridization detects *OsSNF7.2* transcripts in the leaves of 30-d-old plants (B) and the leaf sheaths of 7-d-old seedlings (**C**). Bar, 50 μm. The sense probe of *OsSNF7.2* was used as a negative control (**D**). Bar, 50 μm. (**E**–**I**) β-glucuronidase (GUS) staining of $Pro_{OsSNF7.2}$::GUS transgenic rice plants. *OsSNF7.2* is ubiquitously expressed in the root (**E**), stem (**F**), leaf (**G**), panicle (**H**) and leaf sheath (**I**). Bars, 1 cm. (**J**) Subcellular localization of the OsSNF7.2-GFP (green fluorescent protein) fusion protein in rice protoplasts, using mCherry-VSR2 protein as a prevacuolar compartment (PVC) marker. Bars, 10 μm.

OsSNF7.2. The OsYUC8-GFP fusion protein was expressed in wild-type rice protoplasts, and the fluorescence signals were predominantly detected in the endoplasmic reticulum (ER), as revealed using an ER marker (Figure 6A). Moreover, punctate signals that partly overlapped with the late-endosome marker mCherry-VSR2 were also detected in the protoplasts (Figure 6C). The relationships between OsYUC8-GFP and the ER or prevacuolar compartment (PVC) marker signals were determined by calculating the Pearson's correlation coefficient (French et al., 2008). A confocal microscopy

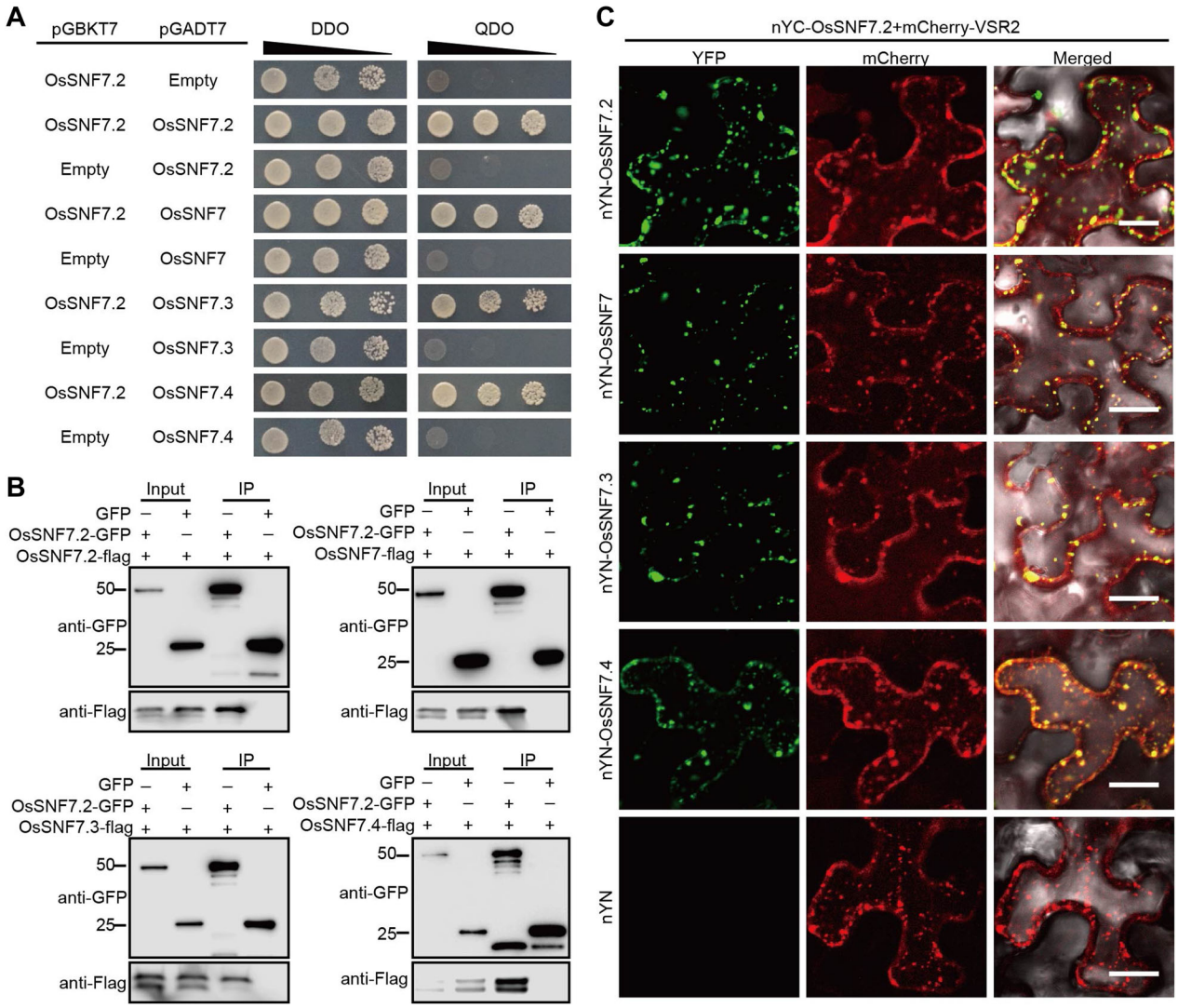

Figure 4. OsSNF7.2 interacts with its protein homologs

(**A**) Yeast two-hybrid assays showing the interactions between OsSNF7.2 and its homologs. Transformed yeast cells were plated on DDO (SD/-Trp/-Leu) and QDO (SD/-Trp/-Leu/-His/-Ade).(**B**) Co-immunoprecipitation (Co-IP) assays using anti-GFP (green fluorescent protein) agarose beads to validate the interactions between OsSNF7.2 and its homologous proteins in rice protoplasts. The symbols "+" and "-" represent the presence and absence of the protein in each sample.(**C**) Bimolecular fluorescent complementation (BiFC) assays of the interaction between OsSNF7.2 and its protein homologs were performed in *Nicotiana benthamiana* leaves. Bars, 20 μm.

analysis showed a strong correlation between OsYUC8-GFP and the ER marker signals ($r_s = 0.763$) and a weaker correlation with the PVC markers ($r_s = 0.438$) in the wild-type protoplasts. By contrast, the OsYUC8-GFP showed a strong correlation with the PVC markers ($r_s = 0.683$) in the *rl17* mutant protoplasts (Figure 6B, D). These data suggest that the OsYUC8-GFP fusion protein was trafficked to the endosomal membrane, and its subcellular localization can be altered by OsSNF7.2.

We speculated that OsYUC8-GFP could be transported through the ESCRT pathway for degradation. We could not detect the GFP signal in *OsYUC8-GFP* transgenic plants, so rice protoplasts expressing related proteins were used for the detection of OsYUC8 degradation. An IP assay was performed using rice protoplasts expressing OsYUC8-GFP, or GFP as a negative control. Both the ubiquitinated form of OsYUC8-GFP and the GFP core (less than 27 kDa), which is a characteristic of vacuolar degradation products for vacuolar delivery of GFP fusion proteins (DaSilva et al., 2005; Scheuring et al., 2012), were detected in the input and IP samples by immunoblotting using anti-GFP and anti-Ubi (P4D1) antibodies. As shown in the left panel of Figure 6E, the GFP core was slightly degraded from the OsYUC8-GFP fusion protein, and was enriched in the IP sample. Also, the ubiquitination of OsYUC8-GFP was found in the form of high-molecular weight smears (Figure 6E, right panel). These results indicate that OsYUC8 can be modified by ubiquitination for vacuolar degradation *in vivo*.

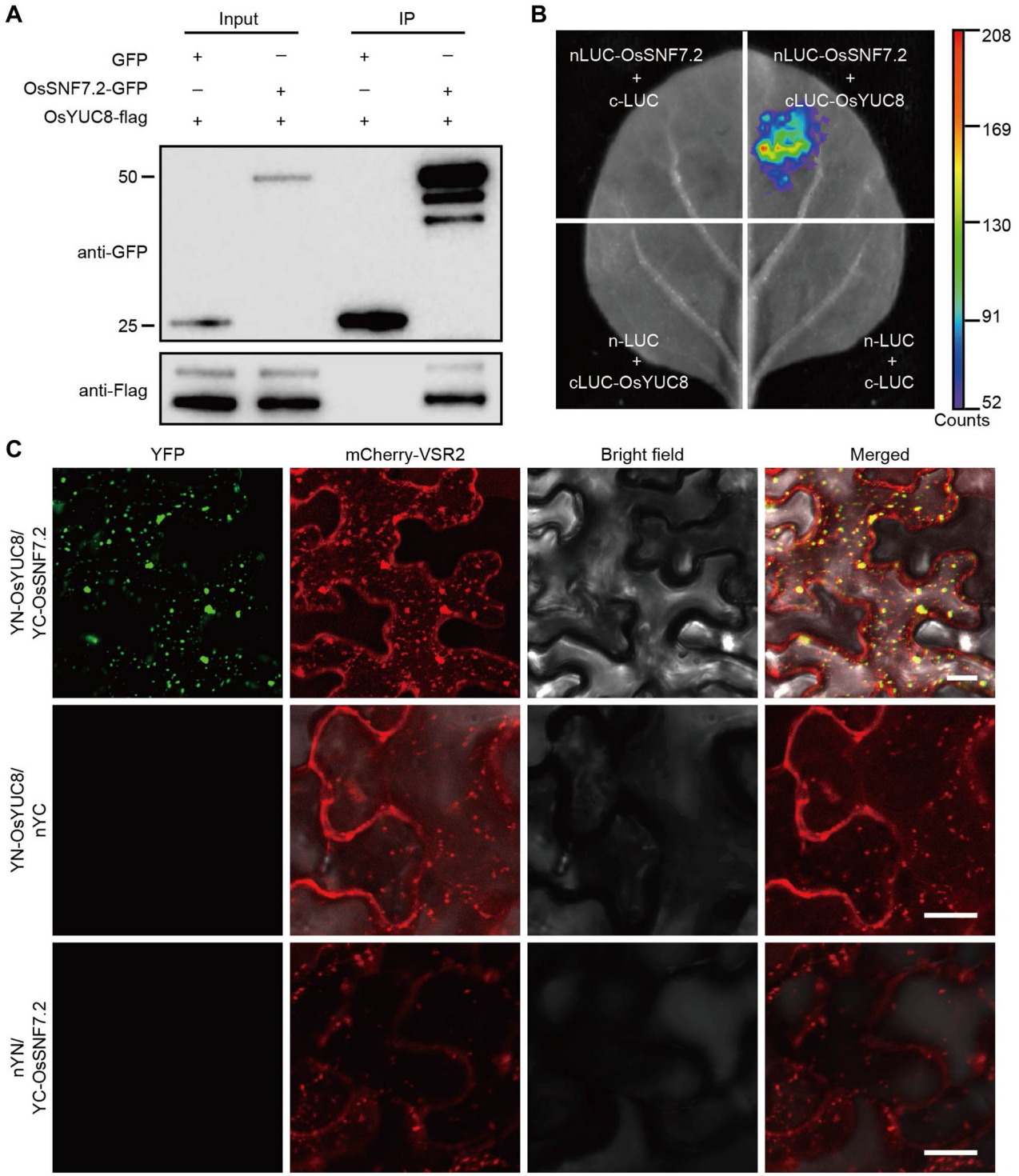

Figure 5. OsSNF7.2 interacts with OsYUC8

(**A**) *In vivo* Co-immunoprecipitation assay using anti-GFP (green fluorescent protein) agarose beads, showing that OsYUC8-Flag was co-immunoprecipitated in rice protoplasts expressing OsSNF7.2-GFP but not free GFP. (**B**) Luciferase complementation imaging (LCI) assay verifying the interaction between OsSNF7.2 and OsYUC8 in *Nicotiana benthamiana* leaves. (**C**) Bimolecular fluorescent complementation (BiFC) assay showing OsYUC8 associated with OsSNF7.2 in mCherry-VSR2-labeled multivesicular body (MVB) compartments in *N. benthamiana* leaves. Bars, 20 μm.

To confirm the degradation of OsYUC8 in the vacuoles, the total proteins were isolated from the protoplasts expressing OsYUC8-GFP in the *rl17* mutant and the wild-type at different timepoints. The GFP core generated by the degradation of the OsYUC8-GFP fusion protein was detected. The GFP core protein emerged at 6 h and accumulated at 8 h in wild-type protoplasts, as shown in Figure S9, whereas no GFP core was detected in the *rl17* mutant during

the entire sampling time. To further confirm the vacuolar degradation of OsYUC8, the protoplasts expressing OsYUC8-GFP were treated with E64D, an inhibitor of cysteine protease that stabilizes proteins in the vacuolar compartment. The GFP core disappeared in both protoplasts after the E64D treatment (Figure 6F). All these data implied that OsSNF7.2 can mediate OsYUC8 degradation in the vacuole.

Concanamycin A (Conc A), a vacuolar-type adenosine triphosphatase inhibitor, can prevent vacuolar hydrolase activity by raising the pH in the vacuolar lumen (Yoshimoto et al., 2004; Gao et al., 2015). To explore whether the absence of the fluorescent OsYUC8-GFP signal in the transgenic plants was due to its vacuolar degradation, we checked the fluorescent signal of OsYUC8-GFP in the radicle of the transformed seedlings in the wild-type background. Obvious signals were detected after the treatment with 0.5 μmol/L Conc A, which suggested that OsYUC8-GFP could be located in the vacuole (Figure S10A). Our immunoblot analysis of OsYUC8-GFP in the transgenic plants treated with dimethyl sulfoxide (DMSO) or Conc A also showed the same results. Before the Conc A treatment, a weak or no protein stripe was detected, while an obvious stripe was detected after treatment with 0.5 μmol/L Conc A (Figure S10B). This result provides further evidence that OsYUC8-GFP is degraded in the vacuole.

OsSNF7.2 and OsYUC8 function in the same pathway to regulate leaf rolling

The mutants *Osyuc8* and *rl17 Osyuc8*, generated by CRISPR/Cas9 genome editing in the Asominori background, were used to further verify the relationship between OsSNF7.2 and OsYUC8 in the pathway regulating leaf rolling. All *Osyuc8* and *rl17 Osyuc8* lines showed an obvious rolled and narrower leaf phenotype, which was more severe in the *rl17 Osyuc8* double mutant (Figure 7A, B). A microscopic examination of leaf cross-sections showed that the rolled phenotypes of *Osyuc8* and *rl17 Osyuc8* resulted from the reduced number and size of bulliform cells (Figure 7C–F). These findings suggest that OsSNF7.2 and OsYUC8 function in the same pathway to regulate leaf rolling.

DISCUSSION

Rice yield is affected by the photosynthetic efficiency of the plant. Leaves are essential organs for photosynthesis, and their size or shape directly affects the photosynthetic efficiency; thus, it is important to study the yield-affecting mechanisms of leaf development. Here, we cloned and characterized the *rl17* mutant, the leaves of which are adaxially rolled due to the decreased number and size of the bulliform cells (Figure 2). The *RL17* allele encodes a vacuolar protein-sorting-associated protein, OsSNF7.2, which is a subunit of the ESCRT-III complex. Through GUS staining, *OsSNF7.2* was found to be constitutively expressed, including in the leaf and stem tissues (Figure 3A, E–I). An *in situ* hybridization clarified that the *OsSNF7.2* mRNA signal was detected in the epidermal cells of the primary leaf (Figure 3C) and the mesophyll cells of mature leaf, with no obvious signal in the bulliform cells (Figure 3B). As bulliform cells are highly specialized cells derived from epidermal cells, we speculate that OsSNF7.2 may function in the epidermal cells of the primary leaf to affect the differentiation of the bulliform cells. Our data showed that OsSNF7.2 interacts with homologous proteins and functions as a multimer; however, only the mutation of *OsSNF7.2*, not its homologous partners, led to leaf rolling (Figure S4). This is the first report that a component of the ESCRT-III complex controls leaf rolling. The ESCRT complex is known to function in the biogenesis of the MVBs and the degradation of their cargoes in the vacuole or lysosome. Previous studies reported that OsYUC8/OsCOW1 functions as an enzyme in auxin biosynthesis and controls leaf rolling by regulating the size of bulliform cells (Woo et al., 2007), but how OsYUC8 controlled leaf rolling was unclear. Our data show that OsSNF7.2 can interact physically with OsYUC8 (Figure 5), as well as other members of the YUC family that might be potential substrates for OsSNF7.2-mediated degradation (Figure S8). OsYUC8 protein was localized in the ER and PVCs (Figure 6) and partially colocalized with OsSNF7.2 in tobacco (Figure S11). OsYUC8 as a cargo protein can be modified by ubiquitination for vacuolar degradation, but the mutation of *OsSNF7.2* interrupted its degradation (Figure 6).

SNF7s are relatively small coiled-coil proteins originally identified by screening for yeast (*Saccharomyces cerevisiae*) mutants unable to grow on sucrose as a carbon source (Tu et al., 1993). The yeast ESCRT-III protein SNF7 participates in *SUC2* expression via the Rim101 pathway (Weiss et al., 2008), a function separated genetically from its functions in endocytic trafficking (Weiss et al., 2009). In yeast, the ESCRT-III subunit VPS20 recruits homo-oligomerization SNF7 capping with VPS24, and VPS24 recruits VPS2 to complete the ESCRT-III complex assembly (Henne et al., 2013). The ESCRT-III protein SNF7 forms spirals at the surface of lipid membranes, which leads to membrane deformation and perhaps membrane scission (Chiaruttini et al., 2015). In *Arabidopsis*, the dominant negative forms of the ESCRT-III SNF7.1 were defective in MVB biogenesis and the vacuolar degradation of membrane proteins (Cai et al., 2014). In the present study, we cloned and elucidated the novel function of *OsSNF7.2* in rice. Although there were numerous homologous genes, only *Ossnf7.2* mutants showed defective leaf development.

Since mutation of *OsSNF7.2* affected vacuolar degradation of OsYUC8, OsYUC8 may be accumulated in the *rl17* mutant, while our data show *Osyuc8* mutant has the similar rolled leaf phenotype as *rl17*. Ubiquitylated cargo is transported to the limiting membrane of the PVCs, with the membrane scission and sequestration of the cargo dependent on the activity of ESCRT-III (Buchkovich et al., 2013). As such a cargo protein, OsYUC8 can be modified by

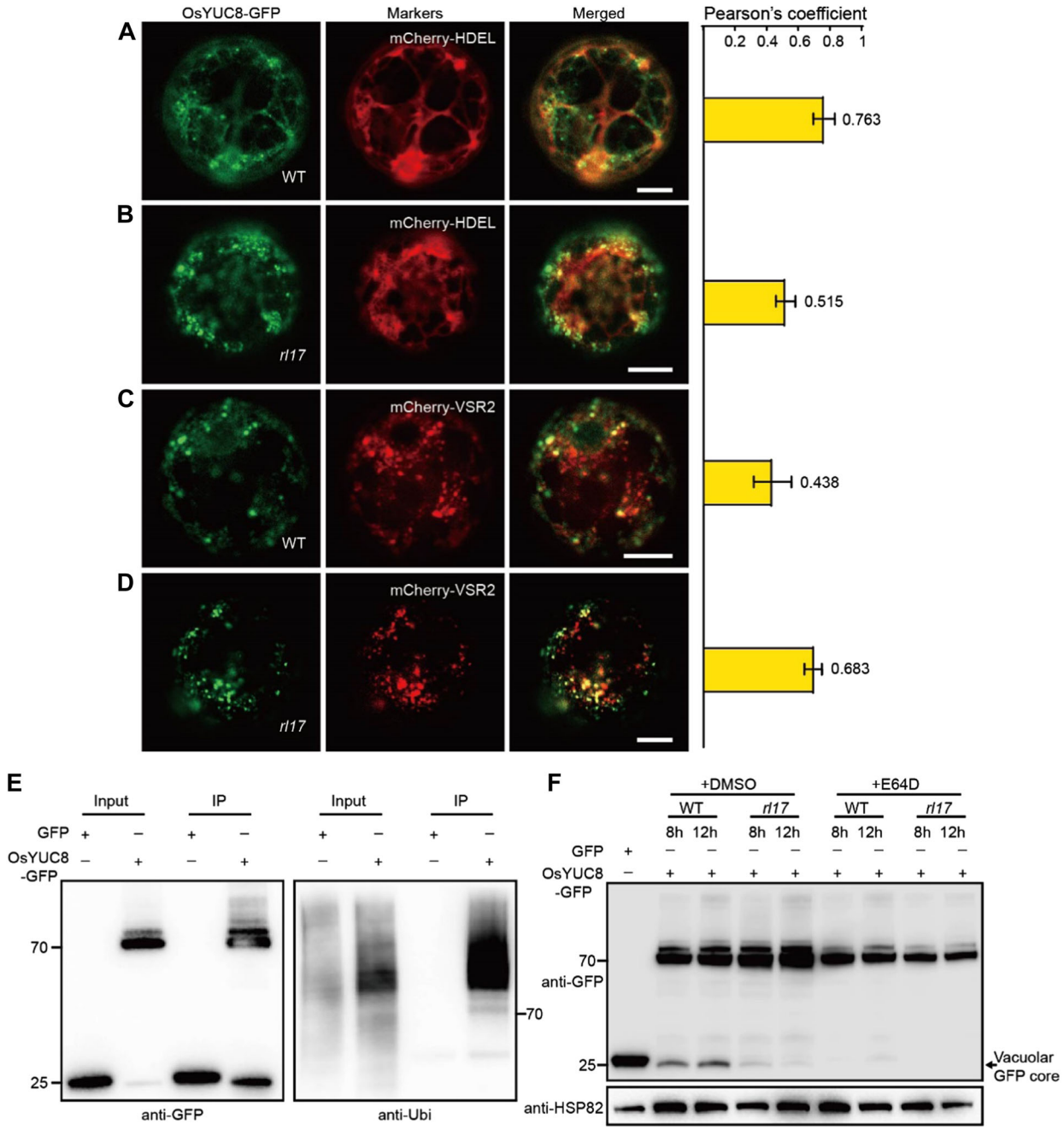

Figure 6. The *rl17* mutant affects the degradation of OsYUC8-GFP (green fluorescent protein)

(**A**) and (**B**) Subcellular localization of the OsYUC8-GFP fusion protein in (**A**) wild-type (WT) and (B) *rl17* mutant rice protoplasts. mCherry-HDEL was used as an endoplasmic reticulum (ER) marker. Bars, 10 μm. Pearson's coefficients between OsYUC8-GFP and each marker are shown in the right pane. Values are means ± *SD*. $n = 6$. (**C**) and (**D**) Subcellular localization of the OsYUC8-GFP fusion protein in (**C**) WT and (D) *rl17* rice protoplasts. mCherry-VSR2 protein was used as a prevacuolar compartment (PVC) marker. Bars, 10 μm. Pearson's coefficients between OsYUC8-GFP and each marker are shown in the right pane. Values are means ± *SD*. $n = 6$. (**E**) IP assay of OsYUC8-GFP. Total proteins were extracted from rice protoplasts expressing GFP or OsYUC8-GFP and subjected to an immunoprecipitation (IP) with GFP-trap. Input protein and IP products were detected using the GFP antibody (left) and anti-Ubi antibody (P4D1) (right). (**F**) Effects of mutated endosomal sorting complex required for transport (ESCRT) component *Ossnf7* on the degradation of OsYUC8-GFP. Proteins were extracted from WT and *rl17* mutant protoplasts expressing OsYUC8-GFP. The OsYUC8-GFP fusion and its degradation products were detected using a GFP antibody with and without E64D treatment.

ubiquitination for vacuolar degradation, which was interrupted in *rl17*, the mutant of *OsSNF7.2*. We showed that *OsYUC8* overexpression did not result in rolled leaves in the transgenic plants, so we hypothesize that the reason for the rolled leaves in *rl17* is not the accumulation of OsYUC8, but the reduction of functional ER-localized OsYUC8 (Figure 6A–D). The knockdown of *OsSNF7.2* suppressed the degradation of OsYUC8 in *rl17*; however, these escaped

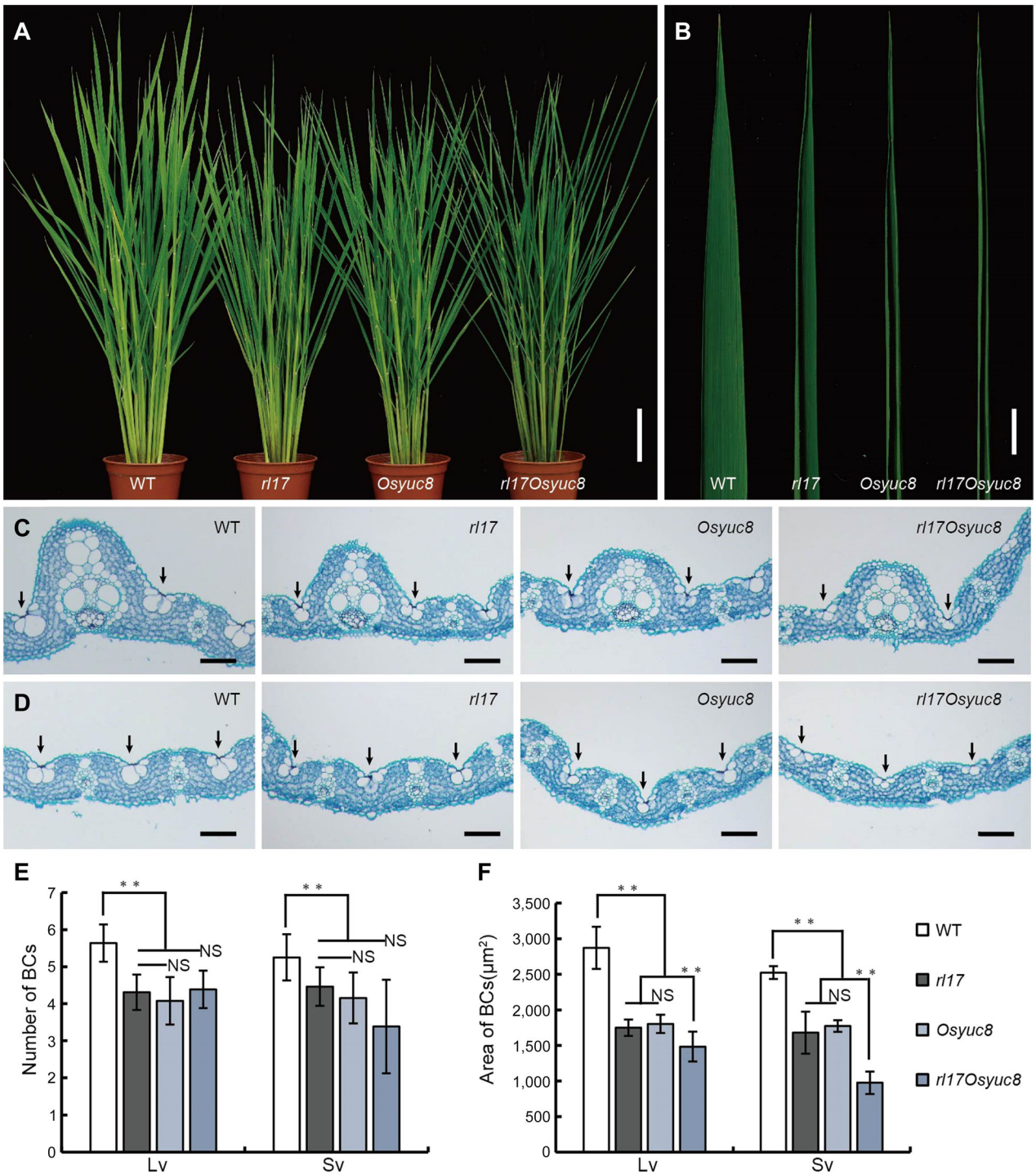

Figure 7. *OsSNF7.2* and *OsYUC8* function in the same pathway to regulate leaf rolling

(**A**) and (**B**) Phenotypes of the wild-type (WT), *rl17*, *Osyuc8*, and *rl17 Osyuc8* plants. All three homozygous knockout genotypes had rolled, narrow leaves. Bars, 10 cm (A), 1 cm (B). (**C**) and (**D**) Cross-sections showing bulliform cells near large veins (C) and small veins (D) in the leaves of 30-d-old knockout plants. The black arrows indicate the bulliform cells. Bars, 100 μm. (**E**) and (**F**) Statistical analyses of number (E) and area (F) of bulliform cells in the WT, *rl17*, *Osyuc8*, and *rl17 Osyuc8* plants. Data are presented as means ± *SD* ($n = 10$, $^{**}P < 0.01$; Student's *t*-tests).

proteins were ubiquitinated (Figure 6E, F) in PVCs, and therefore could not be transported to the ER to perform their normal functions. Although OsSNF7.2 interacts with OsYUC8 to regulate its degradation, functional ER-localized OsYUC8 did not accumulate in *rl17*. The absence of functional OsYUC8 caused the stronger rolled leaves in the *rl17 Osyuc8* double mutant. Alternatively, the more severe rolled-leaf phenotype in the *rl17 Osyuc8* double mutant may

have also been caused by the deficient transportation of other proteins affected by *OsSNF7.2*.

In the ESCRT-dependent protein-sorting pathway, cargoes destined for lysosomal degradation are ubiquitinated and recognized by early-acting ESCRT complexes (ESCRT-0, ESCRT-I, and ESCRT-II), which harbor ubiquitin-binding domains (Schuh and Audhya, 2014). The *Arabidopsis* TOL (TOM1-LIKE) family of ubiquitin-binding proteins recognizes and directly binds to the cargo of the auxin efflux facilitator PIN-FORMED 2 (PIN2) for vacuolar sorting (Korbei et al., 2013). The *Arabidopsis* ESCRT-I component VPS23A, containing an ubiquitin-conjugating enzyme variant (UEV) domain, interacts with PYR1/PYL4 and mediates its delivery to the vacuolar degradation pathway, which helps to regulate the turnover of ABA receptors (Yu et al., 2016). In addition, *Arabidopsis* VPS36, a subunit of ESCRT-II, shows ubiquitin-binding activity and plays important roles in the degradation of ubiquitinated membrane proteins in the vacuoles (Wang et al., 2017). ESCRT-III subunits have no known ubiquitin-binding domains, which deform the limiting membrane and sort the cargo into the intraluminal vesicles of the multivesicular bodies (Henne et al., 2011; Matusek et al., 2014). Whether SNF7 and other ESCRT-III members can interact directly with the ubiquitinated cargoes has not previously been reported; however, here we show that OsSNF7.2 directly binds to OsYUC8 and regulates its sorting into the vacuole for degradation, which gives new insights into the current working model of the ESCRT pathway.

Recent ESCRT-dependent protein degradation studies mostly focused on the ubiquitylation of plasma membrane proteins, with the aim of examining the control of the plasma membrane receptor and transporter abundance in plants. A few plant plasma membrane proteins, such as the PIN2 auxin efflux carrier (Leitner et al., 2012), the FLAGELLIN-SENSING 2 (FLS2) flagellin receptor (Lu et al., 2011), and the BRI1 brassinosteroid receptor (Martins et al., 2015), have been shown to enter the endocytic degradation pathway. Although the ESCRT pathway has long been recognized for its sorting and targeting of integral membrane proteins, the membrane-associated ABA receptors PYL4/PYR1 in *Arabidopsis* interact with FREE1 and VPS23A for endosomal sorting (Belda-Palazon et al., 2016; Yu et al., 2016), while YUC1, a soluble protein, is sorted to vacuolar degradation by unidentified interaction partners (Ge et al., 2019). Recently, the TT3.2 chloroplast precursor protein was shown to be ubiquitinated by the endosome-localized E3 ubiquitin ligase TT3.1, and then sorted into endosomes for vacuolar degradation to maintain the stability of chloroplasts at high temperatures (Zhang et al., 2022). Our study indicated that the ER-localized protein OsYUC8-GFP was sorted to vacuolar degradation by an interaction with the ESCRT machinery component OsSNF7.2, and provided a new degradation process.

MATERIALS AND METHODS

Plant materials and growth conditions

The *rl17* mutant described in this study was isolated from a ^{60}Co-irradiated cultivar Asominori population. A cross between the *rl17* mutant and wild-type Asominori was subjected to a genetic analysis. Rice plants were grown in paddy fields during the normal growing seasons. The LRI of the flag leaves at maturity was calculated as: LRI (%) = (Lw – Ln)/Lw ∗ 100, where Ln and Lw are the blade widths measured under the natural and unfolded states, respectively (Shi et al., 2007).

Histology and microscopy observations

For the paraffin sectioning, the middle parts of the *rl17* mutant and wild-type leaves at the tillering stage were fixed in FAA solution (50% ethanol, 3.7% formaldehyde, and 0.9 mol/L glacial acetic) and treated as previously described (Zhang et al., 2015). The leaves were cut into 8-μm deep cross-sections and were stained with filtered 0.1% toluidine blue before being observed using a light microscope (Leica CTR5000B; Leica Microsystems). The toluidine blue O staining for the characterization of the bulliform cells was performed as previously described (Li et al., 2010), and the bulliform cell areas were determined using Image J software.

Map-based cloning

The *rl17* mutant was crossed with the *indica* variety IR24, and 1,850 $F_{2:3}$ plants with the rolled-leaf phenotype were genotyped using 145 genome-wide simple sequence repeat markers and eight newly developed molecular markers. The molecular markers used for the fine mapping are listed in Table S2.

Vector construction and rice transformation

For the genetic complementation tests, a 5.1-kb genomic DNA fragment containing the 1.2-kb wild-type *OsSNF7.2* coding region, plus 2.1-kb upstream and 1.8-kb downstream regulatory regions, was cloned into the binary vector pCAMBIA1390. The construct was then introduced into a callus derived from the *rl17* mutant using *Agrobacterium tumefaciens*-mediated transformation. To generate *Ossnf7.2* and *Osyuc8* knockout plants, 20-bp gene-specific spacer sequences of *OsSNF7.2* and *OsYUC8* were separately inserted into the single guide RNA (sgRNA)/Cas9 construct (Shan et al., 2013). To obtain *rl17 Osyuc8* double mutants, a CRISPR/Cas9 vector with guide RNAs targeting *OsYUC8* was constructed. The binary constructs were individually introduced into the *Agrobacterium tumefaciens* strain EHA105, and then transformed into calli derived from Asominori and the *rl17* mutant. Homozygous transgenic lines for each knockout were selected using a genotypic identification and sequence alignment. The primers used for the vector construction are listed in Table S2.

RNA extraction and qRT-PCR analyses

Total RNA was extracted from rice tissues using an RNA Prep Pure Plant Kit (Tiangen), then reverse transcribed using PrimeScript II reverse transcriptase and the oligo(dT)18 primer (Takara Bio). qRT-PCR was performed on three biological replicates using a SYBR Premix Ex Taq Kit (Takara Bio) in an ABI Prism 7500 Real-Time PCR System (Thermo Fisher Scientific). The rice *ACTIN1* gene was used as the internal control in all analyses. The primers used for qRT-PCR are listed in Table S2.

Subcellular localization observation and chemical treatments

The full-length coding sequence of *OsSNF7.2* was amplified and fused into the transient expression vector pAN580 to construct Pro_{35S}::OsSNF7.2-GFP, which was transformed into rice protoplasts to investigate the subcellular localization of OsSNF7.2. The methods for rice protoplast preparation and transformation assays were previously described (Zhang et al., 2011). A Zeiss LSM880 confocal microscope (Carl Zeiss) was used to detect the fluorescence signals. The primers are listed in Table S2. For the E64D treatment, the rice protoplasts expressing OsYUC8-GFP were incubated in K3 medium containing 100 μmol/L E64D (Cell Signaling, 10 mmol/L stock in DMSO), or DMSO as the negative control.

For the Conc A treatment, 7-d-old transgenic seedlings of the OsYUC8-GFP transgenic plants in the wild-type background were incubated in 1/2 Murashige and Skoog (MS) medium containing 0.5 μmol/L Conc A for 12 h (FUJIFILM Wako Pure Chemical Corporation; 200 μmol/L stock in DMSO), or with DMSO as the negative control.

RNA *in situ* hybridization

Mid-leaf sections of 30-d-old rice plants were fixed overnight in ribonuclease-free FAA solution at 4°C. After a series of dehydration steps, the samples were embedded in paraffin (Paraplast Plus; MilliporeSigma) before being sectioned. A specific 277-bp complementary DNA (cDNA) fragment was amplified from the *OsSNF7.2* coding region and cloned into the pGEM–T Easy vector (Promega) for the RNA probe preparation. The *in situ* RNA hybridization was performed as previously described (Chen et al., 2015). The primers are listed in Table S2.

Protein interaction assay

A Y2H assay to detect protein interactions was performed using the MatchMaker GAL4 Two-Hybrid System (Takara Bio). The full-length coding sequences of *OsSNF7.2*, *OsSNF7*, *OsSNF7.3*, *OsSNF7.4*, *OsVPS20*, and *OsVPS24* were amplified and cloned into the vectors pGADT7 or pGBKT7 (Takara Bio). Various combinations of constructs were co-transformed into yeast (*Saccharomyces cerevisiae*) strain AH109 following the manufacturer's instructions. Positive transformants were grown on -Trp-Leu (DDO) and -Trp-Leu-His-Ade (QDO) dropout (synthetic defined) plates. The primers used are listed in Table S2.

For the BiFC assays, the full-length coding sequences of the *OsYUC8*, *OsSNF7.2*, and the *OsSNF7.2* homologs were cloned into the binary BiFC vectors pSPYNE173 or pSPYCE (M). The recombinant BiFC vectors were then transformed into the *A. tumefaciens* strain EHA105, and various combinations of the selected strains were co-infiltrated with the P19 strain into 5-week-old *N. benthamiana* leaves, as previously described (Waadt and Kudla, 2008). After 24–48 h, the fluorescence signals were captured using a confocal laser scanning microscope.

For the Co-IP assays, the full-length cDNAs of *OsYUC8*, *OsSNF7.2*, and the *OsSNF7.2* homologs were amplified and cloned into either the pCAMBIA1305–GFP or pCAMBIA1300-3×Flag vectors. Protoplasts isolated from wild-type rice plants were transfected with various plasmid combinations. The polyethylene glycol-mediated transfection and Co-IP assays were conducted as previously described (Zhang et al., 2011; Cai et al., 2021). Western blots were performed with the anti-GFP (11814460001, Roche; 1:2,000), anti-Flag (M185-7, MBL International; 1:5,000), and anti-mouse secondary (D330, MBL International; 1:5,000) antibodies.

For the luciferase (LUC) complementation assays, the full-length coding sequences of *OsYUC8*, *OsSNF7.2*, and the *OsSNF7.2* homologs were cloned into the pCAMBIA-nLUC or pCAMBIA-cLUC vectors. *Agrobacterium* cells harboring various combinations of nLUC and cLUC constructs were co-infiltrated into *N. benthamiana* leaves. The leaves were harvested 2 d later, treated with 1 mmol/L luciferin (E1601; Promega) for 2 min, and the LUC activities were measured using an imaging apparatus (NightShade LB 985, Berthold).

All protein interaction experiments were performed at least three times with similar results.

IP–MS

Rice protoplasts expressing OsSNF7.2-GFP or free GFP were separately homogenized in ice-cold protein extraction buffer containing 0.5 mol/L sucrose, 50 mmol/L Tris-2-[*N*-morpholino]ethanesulfonic acid (pH 8.0), 10 mmol/L ethylenediaminetetraacetic acid (pH 8.0), 1 mmol/L $MgCl_2$, 5 mmol/L dithiothreitol, and 1*Complete Protease Inhibitor Cocktail. The samples were centrifuged at 20 000 *g* for 5 min at 4 °C to remove the cell debris, after which the supernatants were subjected to IP using the m-MACS GFP-tagged protein isolation kit (ChromoTek), following the manufacturer's instructions. The immunoprecipitated proteins were resolved by sodium dodecyl sulfate–polyacrylamide gel electrophoresis, stained with Coomassie brilliant blue (CBB), and then subjected to a MS analysis (Huada Gene Research), as previously described (Ren et al., 2020).

ACKNOWLEDGEMENTS

This research was supported by the Key Laboratory of Biology, Genetics and Breeding of Japonica Rice in the

Mid-Lower Yangtze River, the Ministry of Agriculture, P. R. China, and the Southern Japonica Rice Research and Development Co., Ltd (Nanjing, Jiangsu, China). Funding was also provided by the Jiangsu Science and Technology Development Program (BE2021360), the Natural Science Foundation of Jiangsu Province, Major Project (BK20212010), and the Agricultural Science and Technology Innovation Program of CAAS (CAAS-ZDXT20201, CAAS-ZDXT201903).

CONFLICTS OF INTEREST

The authors declare no conflict of interest.

AUTHOR CONTRIBUTIONS

J.M.W. and S.S.Z. directed the project. J.M.W., S.S.Z., L.Z., and S.H.C. designed the research and wrote the paper. S.H.C. provided the *rl17* mutant material. L.Z. performed most of the experiments. M.H.C., S.C, Y.L.R., X.Y.Z., T.Z.L., and C.L.Z. helped to analyze data. X.J., L.M.Z., M.X.W., and S.Y.Z. helped to generate the transgenic plants. Z.J.C., C.L.L., J.W., and Z.C.Z. conducted the fieldwork. X.Z., X.P.G., Q.B.L., and L.J. provided technical support. All authors read the final manuscript and approved of its content.

Edited by: Liwen Jiang, Chinese University of Hong Kong, China

Received Aug. 17, 2022; **Accepted** Jan. 24, 2023; **Published** Jan. 27, 2023

REFERENCES

Belda-Palazon, B., Rodriguez, L., Fernandez, M.A., Castillo, M.C., Anderson, E.M., Gao, C., Gonzalez-Guzman, M., Peirats-Llobet, M., Zhao, Q., De Winne, N., Gevaert, K., De Jaeger, G., Jiang, L., Leon, J., Mullen, R.T., and Rodriguez, P.L. (2016). FYVE1/FREE1 interacts with the PYL4 ABA receptor and mediates its delivery to the vacuolar degradation pathway. Plant Cell **28:** 2291–2311.

Buchkovich, N.J., Henne, W.M., Tang, S., and Emr, S.D. (2013). Essential N-terminal insertion motif anchors the ESCRT-III filament during MVB vesicle formation. Dev. Cell **27:** 201–214.

Cai, M., Zhu, S., Wu, M., Zheng, X., Wang, J., Zhou, L., Zheng, T., Cui, S., Zhou, S., Li, C., Zhang, H., Chai, J., Zhang, X., Jin, X., Cheng, Z., Zhang, X., Lei, C., Ren, Y., Lin, Q., Guo, X., Zhao, L., Wang, J., Zhao, Z., Jiang, L., Wang, H., and Wan, J. (2021). DHD4, a *CONSTANS-like* family transcription factor, delays heading date by affecting the formation of the FAC complex in rice. Mol. Plant **14:** 330–343.

Cai, Y., Zhuang, X., Gao, C., Wang, X., and Jiang, L. (2014). The *Arabidopsis* endosomal sorting complex required for transport III regulates internal vesicle formation of the prevacuolar compartment and is required for plant development. Plant Physiol. **165:** 1328–1343.

Chen, J., Gao, H., Zheng, X.M., Jin, M., Weng, J.F., Ma, J., Ren, Y., Zhou, K., Wang, Q., Wang, J., Wang, J.L., Zhang, X., Cheng, Z., Wu, C., Wang, H., and Wan, J.M. (2015). An evolutionarily conserved gene, *FUWA*, plays a role in determining panicle architecture, grain shape and grain weight in rice. Plant J. **83:** 427–438.

Chiaruttini, N., Redondo-Morata, L., Colom, A., Humbert, F., Lenz, M., Scheuring, S., and Roux, A. (2015). Relaxation of loaded ESCRT-III spiral springs drives membrane deformation. Cell **163:** 866–879.

DaSilva, L.L.P., Taylor, J.P., Hadlington, J.L., Hanton, S.L., Snowden, C.J., Fox, S.J., Foresti, O., Brandizzi, F., and Denecke, J. (2005). Receptor salvage from the prevacuolar compartment is essential for efficient vacuolar protein targeting. Plant Cell **17:** 132–148.

Fan, L., Li, R., Pan, J., Ding, Z., and Lin, J. (2015). Endocytosis and its regulation in plants. Trends Plant Sci. **20:** 388–397.

Fang, L., Zhao, F., Cong, Y., Sang, X., Du, Q., Wang, D., Li, Y., Ling, Y., Yang, Z., and He, G. (2012). Rolling-leaf14 is a 2OG-Fe (II) oxygenase family protein that modulates rice leaf rolling by affecting secondary cell wall formation in leaves. Plant Biotechnol. J. **10:** 524–532.

French, A.P., Mills, S., Swarup, R., Bennett, M.J., and Pridmore, T.P. (2008). Colocalization of fluorescent markers in confocal microscope images of plant cells. Nat. Protoc. **3:** 619–628.

Gao, C., Zhuang, X., Shen, J., and Jiang, L. (2017). Plant ESCRT complexes: Moving beyond endosomal sorting. Trends Plant Sci. **22:** 986–998.

Gao, C., Luo, M., Zhao, Q., Yang, R., Cui, Y., Zeng, Y., Xia, J., and Jiang, L. (2014). A unique plant ESCRT component, FREE1, regulates multivesicular body protein sorting and plant growth. Curr. Biol. **24:** 2556–2563.

Gao, C., Zhuang, X., Cui, Y., Fu, X., He, Y., Zhao, Q., Zeng, Y., Shen, J., Luo, M., and Jiang, L. (2015). Dual roles of an *Arabidopsis* ESCRT component FREE1 in regulating vacuolar protein transport and autophagic degradation. Proc. Natl. Acad. Sci. U.S.A. **112:** 1886–1891.

Ge, C., Gao, C., Chen, Q., Jiang, L., and Zhao, Y. (2019). ESCRT-dependent vacuolar sorting and degradation of the auxin biosynthetic enzyme YUC1 flavin monooxygenase. J. Integr. Plant Biol. **61:** 968–973.

Henne, W.M., Buchkovich, N.J., and Emr, S.D. (2011). The ESCRT pathway. Dev. Cell **21:** 77–91.

Henne, W.M., Stenmark, H., and Emr, S.D. (2013). Molecular mechanisms of the membrane sculpting ESCRT pathway. Cold Spring Harb. Perspect. Biol. **5:** a01676.

Itoh, J., Nonomura, K., Ikeda, K., Yamaki, S., Inukai, Y., Yamagishi, H., Kitano, H., and Nagato, Y. (2005). Rice plant development: From zygote to spikelet. Plant Cell Physiol. **46:** 23–47.

Korbei, B., Moulinier-Anzola, J., De-Araujo, L., Lucyshyn, D., Retzer, K., Khan, M.A., and Luschnig, C. (2013). *Arabidopsis* TOL proteins act as gatekeepers for vacuolar sorting of PIN2 plasma membrane protein. Curr. Biol. **23:** 2500–2505.

Leitner, J., Petrasek, J., Tomanov, K., Retzer, K., Parezova, M., Korbei, B., Bachmair, A., Zazimalova, E., and Luschnig, C. (2012). Lysine63-linked ubiquitylation of PIN2 auxin carrier protein governs hormonally controlled adaptation of *Arabidopsis* root growth. Proc. Natl. Acad. Sci. U.S.A. **109:** 8322–8327.

Li, L., Shi, Z.Y., Li, L., Shen, G.Z., Wang, X.Q., An, L.S., and Zhang, J.L. (2010). Overexpression of *ACL1* (abaxially curled leaf 1) increased Bulliform cells and induced Abaxial curling of leaf blades in rice. Mol. Plant **3:** 807–817.

Lu, D., Lin, W., Gao, X., Wu, S., Cheng, C., Avila, J., Heese, A., Devarenne, T.P., He, P., and Shan, L. (2011). Direct ubiquitination of pattern recognition receptor FLS2 attenuates plant innate immunity. Science **332:** 1439–1442.

Martins, S., Dohmann, E.M., Cayrel, A., Johnson, A., Fischer, W., Pojer, F., Satiat-Jeunemaitre, B., Jaillais, Y., Chory, J., Geldner, N., and Vert, G. (2015). Internalization and vacuolar targeting of the brassinosteroid hormone receptor BRI1 are regulated by ubiquitination. Nat. Commun. **6:** 6151.

Matusek, T., Wendler, F., Poles, S., Pizette, S., D'Angelo, G., Furthauer, M., and Therond, P.P. (2014). The ESCRT machinery regulates the secretion and long-range activity of Hedgehog. Nature **516:** 99–103.

Moon, J., and Hake, S. (2011). How a leaf gets its shape. Curr. Opin. Plant Biol. **14:** 24–30.

Ren, Y., Wang, Y., Pan, T., Wang, Y., Wang, Y., Gan, L., Wei, Z., Wang, F., Wu, M., Jing, R., Wang, J., Wan, G., Bao, X., Zhang, B., Zhang, P., Zhang, Y., Ji, Y., Lei, C., Zhang, X., Cheng, Z., Lin, Q., Zhu, S., Zhao, Z., Wang, J., Wu, C., Qiu, L., Wang, H., and Wan, J. (2020). GPA5 encodes a Rab5a effector required for post-golgi trafficking of rice storage proteins. Plant Cell **32:** 758–777.

Richardson, L.G., Howard, A.S., Khuu, N., Gidda, S.K., McCartney, A., Morphy, B.J., and Mullen, R.T. (2011). Protein-protein interaction network and subcellular localization of the *Arabidopsis thaliana* ESCRT Machinery. Front. Plant Sci. **2:** 20.

Sasaki Takuji, B.B. (2000). International rice genome sequencing project: The effort to completely sequence the rice genome. Curr. Opin. Plant Biol. **3:** 138–141.

Scheuring, D., Kunzl, F., Viotti, C., Yan, M.S., Jiang, L., Schellmann, S., Robinson, D.G., and Pimpl, P. (2012). Ubiquitin initiates sorting of Golgi and plasma membrane proteins into the vacuolar degradation pathway. BMC Plant Biol. **12:** 164.

Schuh, A.L., and Audhya, A. (2014). The ESCRT machinery: From the plasma membrane to endosomes and back again. Crit. Rev. Biochem. Mol. Biol. **49:** 242–261.

Shan, Q., Wang, Y., Li, J., Zhang, Y., Chen, K., Liang, Z., Zhang, K., Liu, J., Xi, J.J., Qiu, J.L., and Gao, C. (2013). Targeted genome modification of crop plants using a CRISPR-Cas system. Nat. Biotechnol. **31:** 686–688.

Shi, Z., Wang, J., Wan, X., Shen, G., Wang, X., and Zhang, J. (2007). Over-expression of rice *OsAGO7* gene induces upward curling of the leaf blade that enhanced erect-leaf habit. Planta **226:** 99–108.

Spitzer, C., Reyes, F.C., Buono, R., Sliwinski, M.K., Haas, T.J., and Otegui, M.S. (2009). The ESCRT-related CHMP1A and B proteins mediate multivesicular body sorting of auxin carriers in *Arabidopsis* and are required for plant development. Plant Cell **21:** 749–766.

Tu, J., Vallier, L.G., and Carlson, M. (1993). Molecular and genetic analysis of the *SNF7* gene in Saccharomycescerevisiae. Genetics **135:** 17–23.

Waadt, R., and Kudla, J. (2008). In planta visualization of protein interactions using Bimolecular Fluorescence Complementation (BiFC). CSH Protoc. **2008:** pdb prot4995.

Wang, H.J., Hsu, Y.W., Guo, C.L., Jane, W.N., Wang, H., Jiang, L., and Jauh, G.Y. (2017). VPS36-dependent multivesicular bodies are critical for plasmamembrane protein turnover and vacuolar biogenesis. Plant Physiol. **173:** 566–581.

Weiss, P., Huppert, S., and Kolling, R. (2008). ESCRT-III protein Snf7 mediates high-level expression of the *SUC2* gene via the Rim101 pathway. Eukaryot. Cell **7:** 1888–1894.

Weiss, P., Huppert, S., and Kolling, R. (2009). Analysis of the dual function of the ESCRT-III protein Snf7 in endocytic trafficking and in gene expression. Biochem. J. **424:** 89–97.

Winter, V., and Hauser, M.T. (2006). Exploring the ESCRTing machinery in eukaryotes. Trends Plant Sci. **11:** 115–123.

Woo, Y.M., Park, H.J., Su'udi, M., Yang, J.I., Park, J.J., Back, K., Park, Y. M., and An, G. (2007). Constitutively wilted 1, a member of the rice YUCCA gene family, is required for maintaining water homeostasis and an appropriate root to shoot ratio. Plant Mol. Biol. **65:** 125–136.

Xu, P., Ali, A., Han, B., and Wu, X. (2018). Current advances in molecular basis and mechanisms regulating leaf morphology in rice. Front. Plant Sci. **9:** 1528.

Xu, Y., Kong, W., Wang, F., Wang, J., Tao, Y., Li, W., Chen, Z., Fan, F., Jiang, Y., Zhu, Q.H., and Yang, J. (2021). Heterodimer formed by ROC8 and ROC5 modulates leaf rolling in rice. Plant Biotechnol. J. **19:** 2662–2672.

Xu, Y., Wang, Y., Long, Q., Huang, J., Wang, Y., Zhou, K., Zheng, M., Sun, J., Chen, H., Chen, S., Jiang, L., Wang, C., and Wan, J. (2014). Overexpression of *OsZHD1*, a zinc finger homeodomain class homeobox transcription factor, induces abaxially curled and drooping leaf in rice. Planta **239:** 803–816.

Yoshimoto, K., Hanaoka, H., Sato, S., Kato, T., Tabata, S., Noda, T., and Ohsumi, Y. (2004). Processing of ATG8s, ubiquitin-like proteins, and their deconjugation by ATG4s are essential for plant autophagy. Plant Cell **16:** 2967–2983.

Yu, F., Lou, L., Tian, M., Li, Q., Ding, Y., Cao, X., Wu, Y., Belda-Palazon, B., Rodriguez, P.L., Yang, S., and Xie, Q. (2016). ESCRT-I component VPS23A affects ABA signaling by recognizing ABA receptors for endosomal degradation. Mol. Plant **9:** 1570–1582.

Zhang, H., Zhou, J., Kan, Y., Shan, J., Ye, W., Dong, N., Guo, T., Xiang, Y., Yang, Y., Li, Y., Zhao, H., Yu, H., Lu, Z., Guo, S., Lei, J., Liao, B., Mu, X., Cao, Y., Yu, J., Lin, Y., and Lin, H. (2022). A genetic module at one locus in rice protects chloroplasts to enhance thermotolerance. Science **376:** 1293–1300.

Zhang, J.J., Wu, S.Y., Jiang, L., Wang, J.L., Zhang, X., Guo, X.P., Wu, C.Y., and Wan, J.M. (2015). A detailed analysis of the leaf rolling mutant *sll2* reveals complex nature in regulation of bulliform cell development in rice (*Oryza sativa* L.). Plant. Biol. (Stuttg.) **17:** 437–448.

Zhang, X.Q., Hou, P., Zhu, H.T., Li, G.D., Liu, X.G., and Xie, X.M. (2013). Knockout of the VPS22 component of the ESCRT-II complex in rice (*Oryza sativa* L.) causes chalky endosperm and early seedling lethality. Mol. Biol. Rep. **40:** 3475–3481.

Zhang, Y., Su, J., Duan, S., Ao, Y., Dai, J., Liu, J., Wang, P., Li, Y., Liu, B., Feng, D., Wang, J., and Wang, H. (2011). A highly efficient rice green tissue protoplast system for transient gene expression and studying light/chloroplast-related processes. Plant Methods **7:** 30.

SUPPORTING INFORMATION

Additional Supporting Information may be found online in the supporting information tab for this article: http://onlinelibrary.wiley.com/doi/10.1111/jipb.13460/suppinfo

Figure S1. Phylogenetic analysis of OsSNF7.2

Figure S2. OsSNF7.2 interacts with its homologous proteins in rice

Figure S3. OsSNF7.2 interacts with multiple subunits of the endosomal sorting complex required for transport (ESCRT) complex in rice

Figure S4. Phenotypes of the knockout mutants of the *OsSNF7.2* homologs

Figure S5. Expression of the genes related to leaf rolling in the *rl17* mutant

Figure S6. Identification of OsSNF7.2-interacting proteins using immunoprecipitation – mass spectrometry (IP–MS)

Figure S7. OsYUC8 can physically interact with four rice SNF7 members in rice protoplasts

Figure S8. Co-immunoprecipitation assays validating the interactions between OsSNF7.2 and the rice auxin biosynthetic enzyme YUC members in rice protoplasts

Figure S9. Effects of mutated *OsSNF7.2* on the degradation of OsYUC8-GFP (green fluorescent protein). Proteins were extracted from the wild-type (WT) and *rl17* mutant protoplasts expressing OsYUC8-GFP

Figure S10. Phenotype of OsYUC8-GFP (green fluorescent protein) transgenic plants treated with concanamycin (Conc) A

Figure S11. OsYUC8 partially colocalizes with OsSNF7.2 in transgenic tobacco

Table S1. Agronomic traits of the wild-type (WT) and *rl17* mutant plants under natural long-day (NLD) conditions

Table S2. Primers used in this research

Scan using WeChat with your smartphone to view JIPB online

Scan with iPhone or iPad to view JIPB online